JRDN
Journal of Research and Development on Nanotechnology

X-ray Diffraction Peak Profile Analysis for Determination of Microstructural Properties of Hematite (Fe_2O_3)

Moh. Mualliful Ilmi[a†], Nadya Nurdini[a], Evi Maryanti[a], Pindi Setiawan[b], Ismunandar[a,*]

Received
06 July 2021
Accepted
17 July 2021
Published
21 July 2021

DOI: 10.5614/jrdn.2021.1.1.16667

Hematite (α-Fe_2O_3) nanoparticles have been synthesized by chemical precipitation method and characterized by X-ray diffraction (XRD) study and Transmission Electron Microscopy (TEM). The XRD patterns of calcined powder indicates that the materials exhibited pure phase of hematite with hexagonal wurtzite structure. The crystallite size had been calculated using several methods i.e., Scherrer formula,Williamson-Hall methods, and size-strain plot (SSP) method. The lattice strain of the crystals have also been calculated using those methods. The morphology of the product have been characterized by TEM. There is a good agreement between the crystallite size values obtained by all W–H models (UDM, USDM, UDEDM and SSP models and that obtained by TEM analysis. Among all the methods, SSP method shows highest linear fit with experiment data.

Keywords: XPPA; Microstructure; Crystal size; Williamson-Hall; Stress-strain Plot; Hematite.

Introduction

Hematite (α-Fe_2O_3) nanoparticles is one of the most attractive nanomaterials and has been widely utilized in many scientific and technical applications. Thanks to their thermodynamic stability along with their low cost, non-toxicity, and their exceptional magnetic, electronic, photonic, and optical properties, hematite was thoroughly employed in numerous fields i.e., gas sensors (Cuong et al., 2012), biomedical (Lunin et al., 2020), photoanodes (Ahmed et al., 2018), paints (Ilmi et al., 2020, 2021; Katikaneani et al., 2016; Nurdini et al., 2020), catalysis (Basavegowda et al., 2017), building materials (Amer et al., 2015; Khoshakhlagh et al., 2012), and Li-ion batteries (Yajuan Li et al., 2020).

In most of the cases in nanomaterials (such as hematite NPs), in comparison with their bulk counterparts, nanoscale particles (1-100 nm) usually have remarkable and prospective physical properties different from those of micron size particles (10-100 µm). They exhibit diverse interesting properties including magnetic, optical, and other physical properties as well as surface reactivity that depend on their particle size (Deraz, 2010; He et al., 2008). Hence, for a complete understanding of nanoscale material properties, the calculation of the crystallite size needs to be carried out correctly.

Out of all the methods available for the calculation of crystallite size. Scherrer's method is a well-established method that uses XRD patterns to calculate the average size of crystallites based on the width of the diffraction peak. However, Scherrer's formula provides only a lower bound to the crystallite size and overlooks the peak broadening contributions from other important factors such as inhomogeneous strain and instrumental effects. Therefore, the peak broadening resulting from these factors was zero, and then the peak width would be determined solely by the crystallite size.

In fact, both crystallite size and lattice strain possess their own contribution to x-ray diffraction peak broadening in nanomaterials. The peak broadening contributed by lattice strain is owing to the large volume of grain boundaries (Venkateswarlu et al., 2010). Thus, the strain present in the nanomaterials may affect the crystallite size calculation. Therefore, in order to measure the crystallite size correctly and to study the modifications introduced by strain in the properties of nanomaterials, strain calculations are required (Biju et al., 2008).

Unlike Scherrer's method, XPPA (X-ray diffraction peak profile analysis) takes into account peak broadening results from those above mentioned other important factors. This method has been widely used to calculate the grain size, lattice distortion, twinning, stacking fault probabilities, and long-range and root mean square stresses in nanocrystalline materials. Various XPPA analytical methods are being used to estimate the crystallite size and lattice strain present in the material from x-ray peak broadening such as Williamson-Hall methods, Stress-Strain Plot Methods, and Halder-Wagner Methods (Warren et al., 1951; Williamson and Hall, 1953).

This study aims to calculate the crystallite size of nanocrystalline calcined hematite particles more accurately from powder x-ray diffraction data by considering the contributions of other important factors, namely instrumental and lattice strain effects to the x-ray peak broadening. In addition, other microstructural parameters such as lattice strain, lattice deformation stress, and deformation energy density present in the nanoparticles were estimated based on XPPA methods i.e., Williamson-Hall plots using UDM, USDM, UDEDM models, and Stress-Strain Plot Model.

[a] *Division of Inorganic and Physical Chemistry, Institut Teknologi Bandung, Jl. Ganesha no.10, Bandung 40132, Indonesia*
[b] *Division of Visual Communication and Multimedia, Institut Teknologi Bandung, Jl. Ganesha no. 10, Bandung 40132, Indonesia*
* Corresponding author: ismu@chem.itb.ac.id

The crystallite size estimated from x-ray diffraction data is further compared with particle size distribution obtained from TEM analyses.

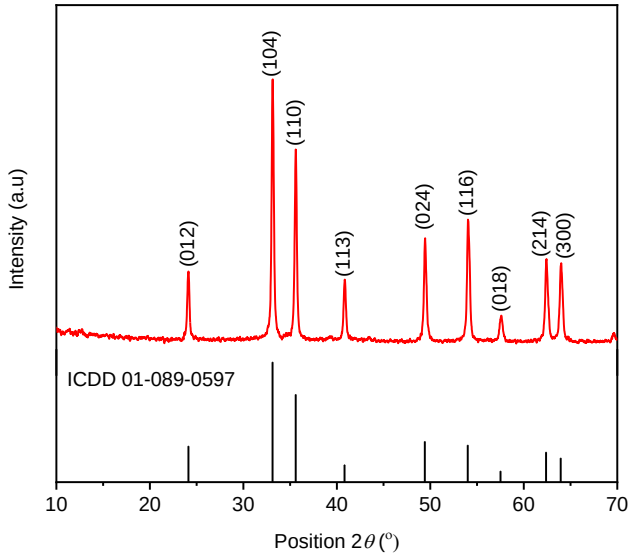

Figure 1. XRD pattern of Hematite nanoparticles with reference

Materials and Experimental

Precipitation technique was used to prepare a fresh paste of iron (III) hydroxide through dropwise neutralization of iron (iii) nitrate hexahydrate ($Fe(NO_3)_3.6H_2O$) solution (1M) with ammonia (NH_4OH) solution at 80 °C with continuous stirring using a magnetic stirrer for 3 hours. After cooled down, the precipitate was left to settle down then centrifuged at 6000 rpm for 15 minutes. The obtained red paste was then washed several times with DI water, diluted ethanol solution until the pH reaches 7. The precipitate was dried in an oven at 80 °C for 24h then calcined in a muffle furnace at 900 °C for 4 h.

The crystal properties of the prepared sample were investigated by X-ray diffraction analysis (XRD) using instrumental D8 ADVANCE, Bruker, Germany. The data were recorded at 2θ between 10° to 70° by 0.02 step, with a scan step time of 0.1 s. The samples were ground using agate mortar before measurement. Crystal phase analysis was performed using Highscore PAN Analytical and compared with references (standard ICDD card no. 01-089-0597). Micrographic images were obtained using TEM HT7700. The data was collected by employing an accelerated voltage of 120 kV.

Results and discussion

3.1. XRD Analysis

The X-ray diffraction (XRD) profile of synthesized hematite nanoparticles is shown in **Figure 1**. The Diffraction pattern demonstrates peaks at 24.12, 33.14, 35.60, 40.85, 49.45, 54.0, 57.5, 62.44, and 64.00, corresponding to the planes of (012), (104), (110), (113), (024), (116), (018), (214), and (300). Those several peaks match with the stick pattern of hexagonal hematite nanocrystal in the International Crystallographic Diffraction Data (ICDD) having no. 01-089-0597. The diffractogram also demonstrated the absence of any impurity. The sharp diffraction peaks indicate the high crystallinity of the prepared particles. From this diffraction profile, we then calculate the crystallite size, intrinsic strain, and stress of the crystal using several models as described in the following section.

3.2. Scherrer's method

X-ray diffraction peak gets broaden in the nanocrystals due to the crystalline size effect and intrinsic strain effect. This phenomenon normally comprises two parts physical broadening and instrumental broadening. The last can be corrected using the following equation,

$$\beta_{hkl}{}^2 = \beta_{exp}{}^2 - \beta_{ins}{}^2 \quad (1)$$

Where β_{hkl} is the corrected broadening, β_{exp}corresponds to experimental broadening, and β_{ins} is the instrument broadening. Here, the crystalline silicon wafer has been employed as a standard reference material for both position calibration and instrumental broadening calculation. Those broadening factors have been measured as full width at half maximum (FWHM). Using the value of FWHM as the corrected broadening (β_{hkl}) we may calculate the average particle size using Scherrer equation (Aly et al., 2017) as follows:

$$D = \frac{N\lambda}{\beta_{hkl}} \cdot \frac{1}{cos\theta} \quad (2)$$

Here, N is the shape factor (N=0.9), λ is the wavelength (nm) of incident X-ray beam (λ of CuKα = 0.154 nm), β_{hkl} is corrected broadening (FWHM) of the corresponding peak, θ is the Bragg diffraction angle (°), and D is the average crystalline size (nm).

Generally, Scherrer method is applied on the diffraction peak which reflects the preferential crystallographic orientation of the crystal (Bagheri-Mohagheghi et al., 2008). Thus, the average crystallite size could be estimated based on the FWHM value of that peak. In hematite case, the preferential orientation is (104) peak positioned at 2θ = 33.14°. By knowing its FHWM value we obtained the average crystallite size = 31. 29 nm.

3.3. Williamson-Hall methods

Since Scherrer formula considers only the effect of crystallite size on the peak broadening. Therefore, it does not provide any information regarding the microstructure of the lattice i.e., the intrinsic strain, which presents in the nanocrystals due to the point defect, grain boundary, triple junction and stacking faults. There are several methods i.e., Williamson Hall (W-H) methods, Stress-Strain Plot (SSP) method, those consider the contribution of the effect of the strain induced XRD peak broadening and can be used for the calculation of the intrinsic strain along with the particle size (Williamson and Hall, 1953). Among these methods, W-H model is a very easy and simplified one. According to W-H model, the total broadening can be expressed as,

$$\beta_{total} = \beta_{size} + \beta_{strain} \quad (3)$$

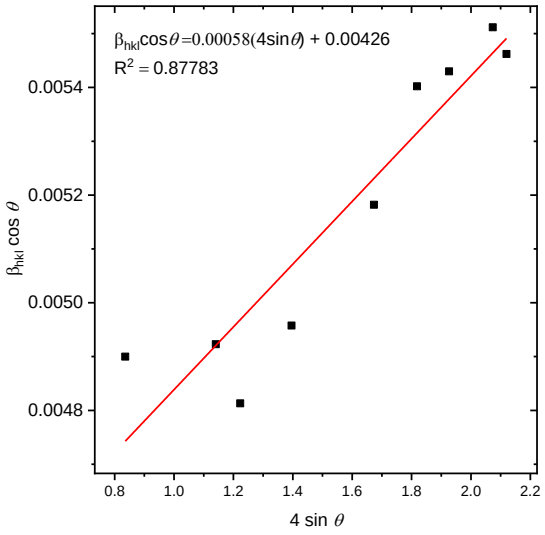

Figure 2. UDM plot for hematite nanoparticles.

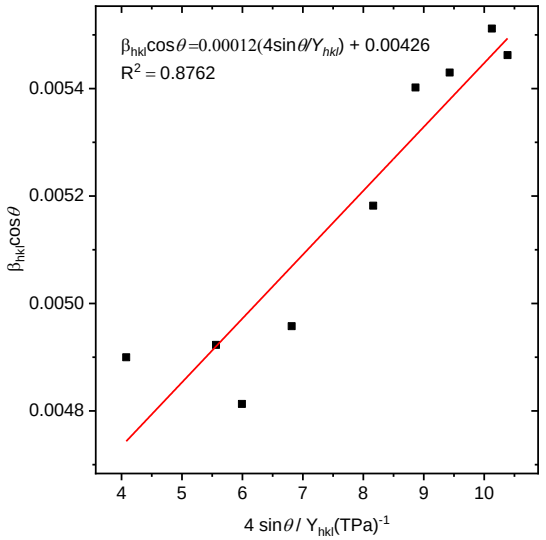

Figure 3. USDM plot for hematite nanoparticles.

W-H model could be divided into three different approximations. In this work, we employed the entire three models to calculate the average particle size and the microstrain of hematite crystal. Here, we also discussed what the fittest model for our material is.

3.3.1 Uniform deformation model (UDM)

The Williamson-Hall UDM model assumes the uniformity of crystal strain along the crystallographic direction. This applied to the broadening of the observed peak from the diffraction patterns owing to the crystal defects. Defects may be imperfections and distortions. This strain (ε) induced XRD peak broadening is given by,

$$\beta_{strain} = 4\varepsilon tan\theta \text{ or } \varepsilon = \frac{\beta_{strain}}{4tan\theta} \quad (4)$$

Since, the size and strain are the factors affect the broadening of a particular peak having the hkl value. Thus, the total peak broadening is simply written as,

$$\beta_{hkl} = \beta_{size} + \beta_{strain} \quad (5)$$

Where β_{hkl} is the FWHM of the peak with particular hkl value. By using eqs. (5), then substituting the β_{size} and β_{strain} with eqs. (2) and (3), respectively. We get (Shunmuga Sundaram et al., 2020),

$$\beta_{hkl} = \frac{N\lambda}{D} \cdot \frac{1}{cos\theta} + 4\varepsilon tan\theta \quad (6)$$

The eqs. (6) then could be rearranged as follows,

$$\beta_{hkl}cos\theta = \frac{N\lambda}{D} + 4\,\varepsilon\, sin\theta \quad (7)$$

Equation (7) is a linear equation and is known as the UDM equation which considers the uniformity of crystal strain in all crystallographic directions. This model expected that the crystal possesses an isotropic nature. **Figure 2** exhibited the UDM plot of all the observed diffraction peaks with 4sinθ along x-axis and $\beta_{hkl}cos\theta$ values along y-axis. The y intercept of the plot allows us to calculate the crystallite size (D) of the crystal, and the slope of the straight line gives the lattice strain (ε) value. Hence, from the intercept, we obtained the average crystallite size as 34.66 nm, whereas, from the slope, the intrinsic strain has been calculated as 0.8×10^{-3}.

3.3.2 Uniform deformation stress model (UDSM)

The expectation of homogenous and isotropic in nature of the crystal as assumed in UDM model is not actually satisfied in several cases. Therefore, as a crystal is possibly anisotropic, W-H equation needs to be modified by substituting more suitable term of the ununiform of strain (ε) value.

Thanks to the Hook's law,

$$\sigma = Y_{hkl}\varepsilon \quad \text{or} \quad \varepsilon = \frac{\sigma}{Y_{hkl}}, \quad (8)$$

where σ is stress, ε is anisotropic micro strain, and Y is young's modulus of particular hkl plane of the hexagonal crystal which can be calculated using the following formula (Balzar et al., 1993; Warren et al., 1951):

$$Y_{hkl} = \frac{\left[h^2 + \frac{(h+2k)^2}{3} + \left(\frac{al}{c}\right)^2\right]^2}{S_{11}\left(h^2 + \frac{(h+2k)^2}{3}\right)^2 + S_{33}\left(\frac{al}{c}\right)^4 + (2S_{13} + S_{44})\left(h^2 + \frac{(h+2k)^2}{3}\right)\left(\frac{al}{c}\right)^2} \quad (9)$$

Where h,k,l are Miller indices, a, c are the lattice constants and S_{ij} are elastic compliances of hexagonal hematite which can be calculated using the elastic stiffness constant Cij. The lattice constant (a, c) of this study was obtained from our previous work (Ismunandar et al., 2020). The formula for computing S_{11}, S_{33}, S_{13}, and S_{44} are shown below (Yan Li and Thompson, 1990; Papaconstantopoulos and Mehl, 2005):

$$S_{11} = \frac{1}{2}\left(\frac{C_{33}}{C_{33}(C_{11}+C_{12}) - 2(C_{13})^2} + \frac{1}{C_{11}-C_{12}}\right) \quad (10)$$

$$S_{33} = \frac{C_{11}+C_{12}}{C_{33}(C_{11}+C_{12}) - 2(C_{13})^2} \quad (11)$$

$$S_{13} = -\frac{C_{13}}{C_{33}(C_{11}+C_{12}) - 2(C_{13})^2} \quad (12)$$

$$S_{44} = \frac{1}{C_{44}} \quad (13)$$

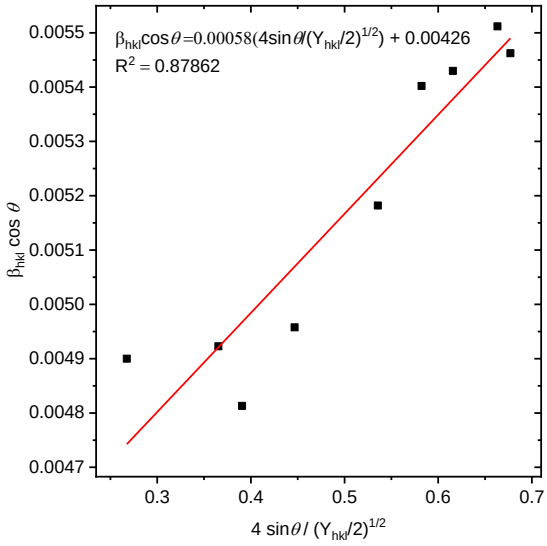

Figure 4. UDEDM plot for hematite nanoparticles.

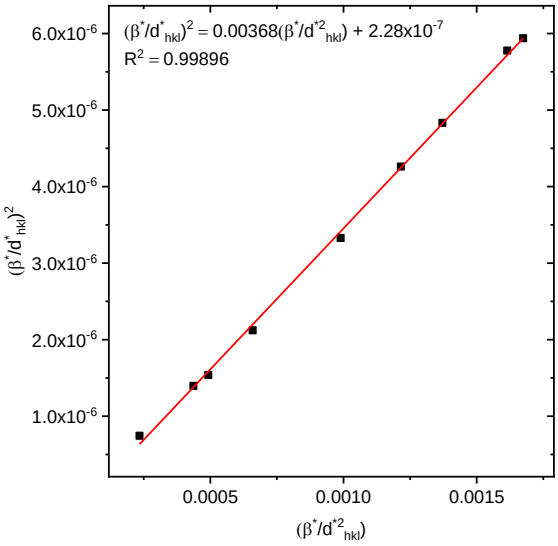

Figure 5. SSP plot for hematite nanoparticles.

As the value of C_{11}, C_{12}, C_{13}, C_{33}, and C_4 are known from the reference (Gaillac et al., 2016). Thus, we could compute each value of the elastic compliance constants as high as $S_{11} = 4.9 \times 10^{-12}$ m^2N^{-1}, $S_{33} = 4.9 \times 10^{-12}$ m^2N^{-1}, $S_{13} = 1.5 \times 10^{-12}$ m^2N^{-1}, $S_{44} = 12.7 \times 10^{-12}$ m^2N^{-1}, respectively.

Employing the Hook's law (eqs. 9), where stress is considered uniform along all the lattice direction, at the same time the strain value is varying depends to the young's value of particular crystallite plane, The USDM W-H linear equation can be written as follows (Pandiyarajan and Karthikeyan, 2012):

$$\beta_{hkl}cos\theta = \frac{N\lambda}{D} + \frac{4\ \sigma\ sin\theta}{Y_{hkl}} \quad (14)$$

By Plotting eqs. (14), with $\beta_{hkl}cos\theta$ along y-axis and $4\ \sigma\ sin\theta/Y$ along x-axis corresponding to each peak in the diffractogram, we could obtain a straight-line plot (**Figure 3**) where the y intercept gives the crystallite size (D) meanwhile; the slope of the line equation gives the uniform deformation stress (σ). By entering the value of the Young's modulus (Y) of hematite, the lattice strain can be obtained. The average particle size and the uniform stress deformation model are approximately as 32.24 nm and 100.0 MPa, respectively.

3.3.3 Uniform deformation energy density models (UDEDM)

Improving the limitation of UDM and USDM models where isotropic nature and linear correlation of stress and strain are almost rare in real crystals, the UDEDM model was introduced to take all the different microstructures of the crystal into account. This model considers the uniform anisotropic lattice strain in all crystallographic directions as the effect of density of deformation energy (Mote et al., 2012).

According to Hook's law where the energy density is related to the strain as written below,

$$u = \frac{\varepsilon^2 Y_{hkl}}{2} \text{ or } \varepsilon^2 = \frac{2u}{Y_{hkl}} \quad (15)$$

by rearranging the eqs. (15) into $\varepsilon = \sqrt{\frac{2u}{Y_{hkl}}}$ and putting the value of ε into eqs. (7) we could obtain the UDEDM expression (Dey and Das, 2018),

$$\beta_{hkl}cos\theta = \frac{N\lambda}{D} + 4\ sin\theta \left(\frac{2u}{Y_{hkl}}\right)^{1/2} \quad (16)$$

Linear plot of the eqs. (16), between $\beta_{hkl}cos\theta$ against $4\ sin\theta \left(\frac{2u}{Y_{hkl}}\right)^{1/2}$ for each corresponding XRD peaks is shown in **Figure 4**. The uniform lattice deformation energy u is estimated from the slope of the linear fit of the plot, whereas the crystallite size (D) is extracted from its intercept. Here, the stress (σ) value was calculated by putting eqs. (8) into eqs. (15) as described below,

$$\sigma = Y_{hkl}\sqrt{\frac{2u}{Y_{hkl}}} \quad (17)$$

By knowing the Young's modulus (Y), then, the lattice strain (ε) can be calculated. The intercept of the plotted straight line provides the average of crystallite size of 32.24 nm, whereas the slope gives the energy density of 52.9 KJm^{-3}. The calculated stress from eqs. (17) was 111.05 MPa.

3.4 Stress-Strain Model

The Williamson-Hall plot models assumed that the line broadening was essentially isotropic. This indicates that the diffraction domains were isotropic as it is due to the contribution of the microstrain. In the cases of isotropic line broadening, an average size-strain plot (SSP) method is applicable to be used for better evaluating the size and strain values of the NPs. This method uses the data prominently from the lower angles and gives relatively less weight gain to the data related to the peaks at higher angle reflection since it usually lacks of accuracy. This method assumed that the crystallite size profile is described by Lorentzian function

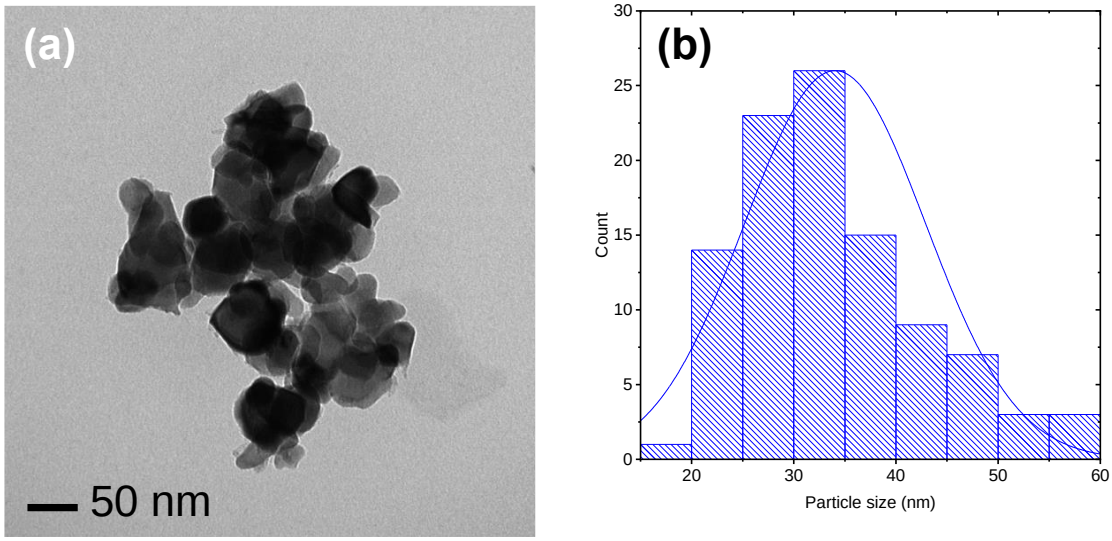

Figure 6. (a) HRTEM image and (b) Grain size distribution of hematite nanoparticles.

Table 1. Summary of geometric parameters of the Hematite nanoparticles

Scherrer method	Williamson-Hall method												Size-strain plot					TEM
D (nm)	UDM			USDM				UDEDM					Dv	ε		σ (MPa)	R^2	D (nm)
	D (nm)	ε 10^{-3}	R^2	D (nm)	ε 10^{-3}	σ (MPa)	R^2	D (nm)	ε 10^{-3}	σ (MPa)	u_{ed} (KJm^{-3})	R^2		ε 10^{-3}	$\varepsilon_{\rho\mu\sigma}$			
31.29	34.66	0.8	0.878	32.24	0.49	100	0.876	32.24	9.34	111.05	52.9	0.878	31.44	1.58	0.31	113.2	0.999	34.04

while the strain profile is by Gaussian function (Stalick, 1993). Thus we obtained,

$$(d_{hkl}\beta cos\theta)^2 = \frac{N}{D_v}\left(d_{hkl}{}^2\beta cos\theta\right) + \left(\frac{\varepsilon}{2}\right)^2 \quad (18)$$

where N is a shape factor of the particles, D is the crystallite size, and ε is the strain which is related to the root mean square strain (ε_{RMS}).

$$\langle\varepsilon_{RMS}\rangle = \left(\frac{\varepsilon}{2\sqrt{2\pi}}\right) \quad (19)$$

By plotting $(d_{hkl}\beta cos\theta)^2$ on y-axis along with respect to $\left(d_{hkl}{}^2\beta cos\theta\right)$ on x-axis as described in eqs. 18, the corresponding SSP for all diffracting peaks of hematite has been obtained (**Figure 5**). From the plot, the particle size is calculated from the slope of the linearly fitted data and the square root of the y intercept gives RMS strain. The obtained average particle size is 31.44 nm, whilst the calculated intrinsic strain value is 1.58 x 10^{-3}.

3.5 TEM Study

Morphology of hematite nanoparticles has been studied using HRTEM operating at 120 kV of accelerating voltage. (**Figure 6a**) demonstrates the HRTEM image of the hematite nanoparticle, along with the particle-size distribution graph as in **Figure 6b**. The particle-size distribution was obtained from Image-J image processing software. The average particle size obtained from that graph is 34.04 nm and it shows a good agreement with the average particle size obtained from all W-H methods and SSP method.

Conclusions

Pure nanoparticle hematite ($\alpha - Fe_2O_3$) was successfully synthesized using the precipitation method using precursor materials of iron (iii) nitrate hexahydrate ($Fe(NO_3)_2.6H_2O$ and ammonia solution. The summary of the crystallite size and lattice strain calculation among all methods is shown in **Table 1**. The calculated crystallite size using Scherrer analysis exhibited a significant difference compared to obtained crystallite size value by the TEM analysis. On the other hand, there is a good agreement between the crystallite size values obtained by all W–H models (UDM, USDM, UDEDM) and SSP models and those obtained by TEM analysis. Among all the models applied, the SSP model exhibited the highest R square value with the experimental data. Hence, SSP analysis and W-H models result in more accurate estimation of crystallite size compared to Scherrer analysis.

Conflict of Interest

There are no conflicts to declare.

Acknowledgements

This research was funded by Hibah Program Pendidikan Magister Menuju Doktor untuk Sarjana Unggul (PMDSU) Batch IV from the Ministry of Education, Culture, Research and Technology, the Republic of Indonesia. MMI and NN acknowledge the PMDSU

Batch IV scholarship from the Ministry of Education and Culture of the Republic of Indonesia. EM is grateful to the LPDP (Indonesia Endowment Fund for Education) scholarship from the Ministry of Finance, the Republic of Indonesia.

References

Ahmed, A. Y., Ahmed, M. G., Kandiel, T. A. (2018) 'Hematite photoanodes with size-controlled nanoparticles for enhanced photoelectrochemical water oxidation', *Applied Catalysis B: Environmental*, 236, pp. 117–124. doi:10.1016/j.apcatb.2018.04.073

Aly, K. A. *et al.* (2017) 'Estimation of lattice strain for zirconia nano-particles based on Williamson- Hall analysis', *Materials Chemistry and Physics*, 193, pp. 182–188. doi:10.1016/j.matchemphys.2017.01.059

Amer, A. A., El-Sokkary, T. M., Abdullah, N. I. (2015) 'Thermal durability of OPC pastes admixed with nano iron oxide', *HBRC Journal*, 11(2), pp. 299–305. doi:10.1016/j.hbrcj.2014.04.002

Bagheri-Mohagheghi, M.-M. *et al.* (2008) 'The effect of the post-annealing temperature on the nano-structure and energy band gap of SnO2 semiconducting oxide nano-particles synthesized by polymerizing–complexing sol–gel method', *Physica B: Condensed Matter*, 403(13–16), pp. 2431–2437. doi:10.1016/j.physb.2008.01.004

Balzar, D., Roshko, A., Ledbetter, H. (1993) 'X-ray diffraction peak-broadening analysis of (La-M)2Cu04high-Tcsuperconductors', *Powder Diffraction, 8(1), pp. 2-6*. doi:10.1017/S0885715600017656

Basavegowda, N., Mishra, K., Lee, Y. R. (2017) 'Synthesis, characterization, and catalytic applications of hematite (α - Fe 2 O 3) nanoparticles as reusable nanocatalyst', *Advances in Natural Sciences: Nanoscience and Nanotechnology*, 8(2), p. 025017. doi:10.1088/2043-6254/aa6885

Biju, V. *et al.* (2008) 'Estimation of lattice strain in nanocrystalline silver from X-ray diffraction line broadening', *Journal of Materials Science*, 43(4), pp. 1175–1179. doi:10.1007/s10853-007-2300-8

Cuong, N. D. *et al.* (2012) 'Gas sensor based on nanoporous hematite nanoparticles: Effect of synthesis pathways on morphology and gas sensing properties', *Current Applied Physics*, 12(5), pp. 1355–1360. doi:10.1016/j.cap.2012.03.026

Deraz, N. M. (2010) 'Size and crystallinity-dependent magnetic properties of copper ferrite nano-particles, *Journal of Alloys and Compounds'*, 501(2), pp. 317–325. doi:10.1016/j.jallcom.2010.04.096

Dey, P. C. and Das, R. (2018) 'Effect of silver doping on the elastic properties of CdS nanoparticles', *Indian Journal of Physics,* 92, pp. 1099-1108. doi:10.1007/s12648-018-1214-4

Gaillac, R., Pullumbi, P., Coudert, F.-X. (2016) 'ELATE: an open-source online application for analysis and visualization of elastic tensors', *Journal of Physics: Condensed Matter*, 28(27), p. 275201. doi:10.1088/0953-8984/28/27/275201

He, Y. T., Wan, J., Tokunaga, T. (2008) 'Kinetic stability of hematite nanoparticles: the effect of particle sizes', *Journal of Nanoparticle Research*, 10(2), pp. 321–332. doi:10.1007/s11051-007-9255-1

Ismunandar *et al.* (2020) 'Investigation on the Crystal Structures of Hematite Pigments at Different Sintering Temperatures', *Key Engineering Materials,* 874, pp. 20-27. doi:10.4028/www.scientific.net/KEM.874.20

Ilmi, M. M. *et al.* (2021) 'A review of radiometric dating and pigment characterizations of rock art in Indonesia', *Archaeological and Anthropological Sciences*, 13(7), p. 120. doi:10.1007/s12520-021-01357-6

Ilmi, M. M. *et al.* (2020) 'Multi-analytical characterizations of prehistoric rock art pigments from Karim Cave, Sangkulirang–Mangkalihat site, East Kalimantan, Indonesia', *Microchemical Journal*, 155, p. 104738. doi:10.1016/j.microc.2020.104738

Katikaneani, P. *et al.* (2016) 'Phase Transformation of Iron Oxide Nanoparticles from Hematite to Maghemite in Presence of Polyethylene Glycol: Application as Corrosion Resistant Nanoparticle Paints', *Journal of Nanoscience*, 2016, pp. 1–6. doi:10.1155/2016/1328463

Khoshakhlagh, A., Nazari, A., Khalaj, G. (2012) 'Effects of Fe2O3 Nanoparticles on Water Permeability and Strength Assessments of High Strength Self-Compacting Concrete', *Journal of Materials Science & Technology*, 28(1), pp. 73–82. doi:10.1016/S1005-0302(12)60026-7

Li, Y. *et al.* (2020) 'Nitrogen/chlorine-doped carbon nanodisk-encapsulated hematite nanoparticles for high-performance lithium-ion storage', *Journal of Alloys and Compounds*, 843, p. 156045. doi:10.1016/j.jallcom.2020.156045

Li, Y. and Thompson, R. B. (1990) 'Relations between elastic constants C i j and texture parameters for hexagonal materials', *Journal of Applied Physics*, 67(5), pp. 2663–2665. doi:10.1063/1.345479

Lunin, A. V. *et al.* (2020) 'Hematite Nanoparticles from Unexpected Reaction of Ferrihydrite with Concentrated Acids for Biomedical Applications', *Molecules*, 25(8), p. 1984. doi:10.3390/molecules25081984

Mote, V., Purushotham, Y., and Dole, B. (2012) 'Williamson-Hall analysis in estimation of lattice strain in nanometer-sized ZnO particles', *Journal of Theoretical and Applied Physics*, 6(6), pp. 1-8. doi:10.1186/2251-7235-6-6

Nurdini, N. *et al.* (2020) 'Physicochemical investigation of prehistoric rock art pigments in Tewet Cave, Sangkulirang-Mangkalihat Site, East Kalimantan-Indonesia', *Journal of Archaeological Science: Reports*, 31, p. 102345. doi:10.1016/j.jasrep.2020.102345

Pandiyarajan, T., and Karthikeyan, B. (2012) 'Cr doping induced structural, phonon and excitonic properties of ZnO nanoparticles', *Journal of Nanoparticle Research*, 14(647), pp. 1-9. doi:10.1007/s11051-011-0647-x

Papaconstantopoulos, D. A. and Mehl, M. J. (2005) 'Tight-Binding Method in Electronic Structure', *Encyclopedia of Condensed Matter Physics*, Elsevier. doi:10.1016/B0-12-369401-9/00452-6

Sundaram, P. S. *et al.* (2020) 'XRD structural studies on cobalt doped zinc oxide nanoparticles synthesized by coprecipitation method: Williamson-Hall and size-strain plot approaches', *Physica B: Condensed Matter,* 595, p. 412342. doi:10.1016/j.physb.2020.412342

Stalick, J. K. (1993) 'Accuracy in Powder Diffraction-II: A report on the Second International Conference - Gaithersburg, Md - May 26-29, 1992, *Journal of Research of the National Institute of Standards and Technology,* 98(2), pp. 241-244. doi:10.6028/jres.098.019

Venkateswarlu, K., Chandra Bose, A., Rameshbabu, N. (2010) 'X-ray peak broadening studies of nanocrystalline hydroxyapatite by Williamson–Hall analysis', *Physica B: Condensed Matter*, 405(20), pp. 4256–4261. doi:10.1016/j.physb.2010.07.020

Warren, B. E., Averbach, B. L., Roberts, B. W. (1951) 'Atomic Size Effect in the X-Ray Scattering by Alloys', *Journal of Applied Physics*, 22(12), pp. 1493–1496. doi:10.1063/1.1699898

Williamson, G. and Hall, W. (1953) 'X-ray line broadening from filed aluminium and wolfram', *Acta Metallurgica*, 1(1), pp. 22–31. doi:10.1016/0001-6160(53)90006-6

